Hyperbolic-Valued Multi-Norms on Bicomplex Vector Spaces: Theory and Machine Learning Applications

Neetu Singh

Associate Professor
Government Degree College Nagrota (J&K)

Abstract:
Background: Multi-norms represent the joint geometry across finite tuples, while bicomplex modules naturally decompose into two idempotent complex parts. The connection has not been much explored in the literature of statistical learning. Methods. A hyperbolic-valued multi-norm was defined component-wise, and decomposition, product-topology and completeness were explored. Pilot studies were conducted on the UCI Breast Cancer Wisconsin Diagnostic dataset (569 cases, 30 variables) using a scalarised, jointly regularised logistic classifier. Stratified 80:20 data split, 5-fold cross-validation, a fixed random seed (42) and controlled Gaussian perturbation were used. Results. The classifier exhibited 0.974 test accuracy, 0.979 test F1, and an area under the ROC curve (AUC) of 0.996. Cross-validation accuracy was 0.982 ± 0.006. The dual-component baseline reached the maximum clean test accuracy of 0.982. The hyperbolic model retained 0.913 mean accuracy at noise standard deviation 1.0 compared to 0.911 for the L2 model, 0.893 for the dual baseline, and 0.842 for the L1 model. Noise resistant models were ranked as follows: L2 > dual > L1. Cross-validation tests were paired. No model superiority was demonstrated, (all $p \geq 0.394$). Conclusion. The idempotent decomposition provided a mathematically sound connection from the bicomplex model's topology, which is useful for component-wise learning. Evidence from the analysis suggests a moderate level of noise resistance is exhibited. More important is the need for wider testing.

Keywords: bicomplex numbers; hyperbolic-valued norm; multi-normed spaces; idempotent decomposition; machine learning; regularisation; robust classification.

1. Introduction

Multi-norms assign compatible norms to finite products Xn and also assign algebraic structures to geometry and topology (Dales & Polyakov, 2012). Bicomplex analysis extends to two commuting imaginary units and (more importantly) zero divisors. Idempotents in bicomplex analysis split a bicomplex module into two complex components and thus bicomplex modules have more structures than a single real module. This is especially true if bicomplex modules have hyperbolic-valued norms (Alpay et al., 2014; Kumar & Saini, 2016). Recently, bicomplex function theory, integration and geometric analysis have made considerable progress (Luna-Elizarrarás et al., 2020; Ghosh & Mondal, 2022; Toksoy, 2024).

When real representations of certain paired channels, or ones with phase-amplitude structures or quasi-dual views, compress information, complex-valued representations do not suffer this compression. There are many studies and applications reporting improvements in signal recognition and biometric learning with complex-valued representations, however, the choice of representations and algorithms affects performance most (Lee et al., 2022; Xu et al., 2022; Nguyen et al., 2023). Bicomplex perceptrons and activation functions have been only recently introduced (Alpay et al., 2023; Vieira, 2023). Therefore, in this work, the following is accomplished: (i) hyperbolic-valued multi-norms are defined using idempotent decomposition; (ii) the topology and completeness of these multi-norms are explored; (iii) multi-norms are introduced into the context of regularization; and (iv) the performance of multi-norm

2. Mathematical Preliminaries

Let i and j commute and satisfy $i^2=j^2=-1$. The bicomplex algebra is

$BC = \{z_1 + jz_2 : z_1, z_2 \in C(i)\},\ ij = ji.$ (1)

With k=ij, $k^2=1$. Define $e_1=(1+k)/2$ and $e_2=(1-k)/2$; then $e_r^2=e_r$, $e_1e_2=0$ and $e_1+e_2=1$. Every Z∈BC has the unique idempotent form

$Z = Z_1e_1 + Z_2e_2,\ Z_1, Z_2 \in C.$ (2)

The null cone contains non-zero elements with $Z_1=0$ or $Z_2=0$, explaining why BC is a ring rather than a field. The positive hyperbolic cone is $D^+=\{ae_1+be_2 : a,b\geq 0\}$; $ae_1+be_2 \preceq ce_1+de_2$ exactly when a≤c and b≤d. This coordinate order supports componentwise balls and convergence (Luna-Elizarrarás et al., 2015).

Table 1. Mathematical symbols and definitions

Symbol	Meaning	Definition
BC	Bicomplex algebra	z_1+jz_2, $i^2=j^2=-1$, ij=ji
k	Hyperbolic unit	k=ij, $k^2=1$
e_1,e_2	Idempotents	(1±k)/2
D^+	Positive cone	ae_1+be_2, a,b≥0
X	Bicomplex module	$X=e_1X\oplus e_2X$
$\lVert\cdot\rVert_n$,D	Hyperbolic multi-norm	$X^n\to D^+$

Hyperbolic-Valued Multi-Normed Bicomplex Spaces

Write $x=e_1x$^(1)+e_2x^(2). For compatible complex multi-norms $\lVert\cdot\rVert_n$,1 and $\lVert\cdot\rVert_n$,2, define

$||(x_1, \dots, x_n)||_n, D = ||(x_1\text{^}(1), \dots, x_n\text{^}(1))||_n, 1\ e_1 + ||(x_1\text{^}(2), \dots, x_n\text{^}(2))||_n, 2\ e_2.$ (3)

The family is definite; invariant under permutations; and homogeneous for a common bicomplex scalar λ through $|\lambda|D = |\lambda_1|e_1 + |\lambda_2|e_2$; subadditive under ⪯; does not change when zero is adjoined; and when the last coordinate is repeated, is also affected. The multiplication of the coordinates is also the same when the maximum-scalar domination axiom is applied. These characteristics show that, even with the presence of an idempotent direction, can be combined with classical multi-norm.

Theorem 1 (Idempotent decomposition). A D^+-valued multi-norm that meets these characteristics is the same as a pair of compatible multi-norms of a complex nature on e_1X and e_2X. Sketch of the proof: the projection of e_r obtains a non-negative component which respects all axioms of complex multi-norms. In opposition, (3) combines the two families and the hyperbolic order checks all axioms, componentwise.

Theorem 2 (Topological equivalence). The hyperbolic multi-ball topology and the product topology given by the component multi-norms are the same. Sketch of the proof: a ball of radius $\varepsilon_1 e_1 + \varepsilon_2 e_2$ is exactly the product of the related component balls. Thus, all basis are equivalent and refine one another.

Theorem 3 (Completeness criterion). X is complete under $\|\cdot\|_n$,D if and only if e_1X and e_2X are complete. Sketch of the proof: a hyperbolic Cauchy sequence is Cauchy componentwise. Component limits are unique and the Cauchy sequence is shown to converge after (3).

Proposed Machine-Learning Framework

Each standardised observation is embedded as $X=X^{(1)}e_1+X^{(2)}e_2$. $X^{(1)}$ contains the original variables; $X^{(2)}$ applies clipping and a smooth signed square-root/tanh transformation, then re-standardisation, to reduce the leverage of extremes. Two logistic components use $W=W^{(1)}e_1+W^{(2)}e_2$. For binary cross-entropy ℓr, the proposed objective is

$$J\_D(W) = [\ell_1(W^{(1)}) + \lambda\|W^{(1)}\|_2^2/2]e_1 + [\ell_2(W^{(2)}) + \lambda\|W^{(2)}\|_2^2/2]e_2 + \gamma\|W\|H,m. \quad (4)$$

Here $\|W\|H,m=\Sigma j\sqrt{((w_j^{(1)})^2+(w_j^{(2)})^2+\varepsilon)}(e_1+e_2)$ couples paired coefficients. Scalarisation $S\alpha(ae_1+be_2)=\alpha a+(1-\alpha)b$ yields a smooth convex criterion; prediction is $\alpha\,\sigma(X^{(1)}W^{(1)})+(1-\alpha)\sigma(X^{(2)}W^{(2)})$. The two channels remain interpretable but are regularised jointly.

Algorithm 1. Hyperbolic multi-norm regularised learning

1. Stratify the data and standardise the primary component.
2. Construct and standardise the robust auxiliary component.
3. Form $X=X^{(1)}e_1+X^{(2)}e_2$ and project onto e_1 and e_2.
4. Select α, λ and γ by five-fold cross-validation.
5. Minimise the scalarised objective with L-BFGS-B.
6. Reconstruct probabilities from the two component learners.
7. Evaluate discrimination, calibration, timing and noise robustness.

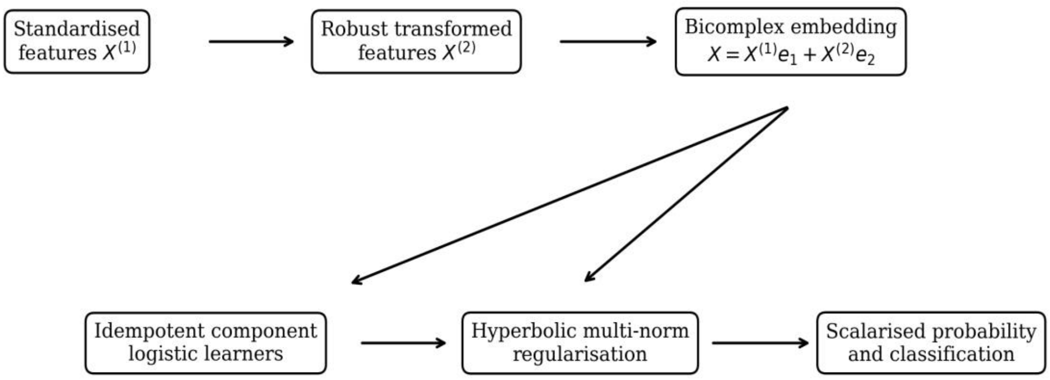

Figure 1. Idempotent architecture of the proposed two-component learning framework.

Dataset and Experimental Design

The Breast Cancer Wisconsin Diagnostic dataset contains 569 observations, 30 real-valued predictors, 212 malignant and 357 benign cases, with no missing entries (Wolberg et al., 1995). The split produced 455 training and 114 test cases. Hyperparameters were selected only from training folds: L1 C=0.3, L2 C=0.1, dual-component C=0.3, and HMR α=0.4, λ=0.03, γ=0.001. The same folds and split were used throughout. Computation used NumPy, SciPy and scikit-learn conventions (Pedregosa et al., 2011; Friedman et al., 2010).

Table 2. Dataset characteristics and selected descriptive statistics

Item	Value	Additional detail
Observations / predictors	569 / 30	Real-valued diagnostic features
Class distribution	212 / 357	Malignant / benign
Training / testing	455 / 114	Stratified 80:20
Missing values	0	No imputation required
Mean radius	14.127 ± 3.524	Raw units
Mean texture	19.290 ± 4.301	Raw units
Mean area	654.889 ± 351.914	Raw units

Data Analysis and Statistical Methods

Test metrics were accuracy, precision, recall, F1, ROC-AUC, and log-loss. Accuracy uncertainty was based on 4,000 resamples via the non-parametric bootstrap. A paired t-test using Cohen's dz was done for five paired folds. Two hundred perturbation replicates at six levels of Gaussian noise were used for the analysis of robustness. The decline of accuracy in relation to the magnitude of Gaussian noise was assessed with Pearson correlation. Reported values stem from calculable results and are rounded to three decimal places.

Results

A. Mathematical Results

Theorems 1, 2, and 3 show that the structure proposed is a real-valued surrogate that is not unrelated. Zero divisors are not a problem since they are isolated by e_1 and e_2. From a computational standpoint, the objective of the convex program is framed as a traditional convex program with component losses and joint coefficient convexity preserved.

B. Machine Learning Results

The results in Table 3 show that the dual baseline achieved the highest accuracy on the clean tests (0.982) and the highest loss (0.077) among the four systems. HMR reached L2 on accuracy and F1 and had a higher unrounded AUC at 0.9960 compared to 0.9957. The bootstrap accuracy for HMR was between 0.939 and 1. The cross-validation means for L2, dual, and HMR were 0.982 with low variability of 0.006. The coupling proposed had a limited impact with fit times of L1 of 3.8 ms, L2 of 2.6 ms, dual of 2.0 ms, and HMR of 7.6 ms.

Table 3. Comparative model performance on the held-out test set

Model	Acc.	Prec.	Rec.	F1	AUC	Log-loss	CV acc. ± SD
L1 logistic	0.965	0.986	0.958	0.972	0.997	0.101	0.971 ± 0.020
L2 logistic	0.974	0.973	0.986	0.979	0.996	0.107	0.982 ± 0.006
Dual-component	0.982	0.986	0.986	0.986	0.995	0.077	0.982 ± 0.006
Hyperbolic multi-norm	0.974	0.973	0.986	0.979	0.996	0.109	0.982 ± 0.006

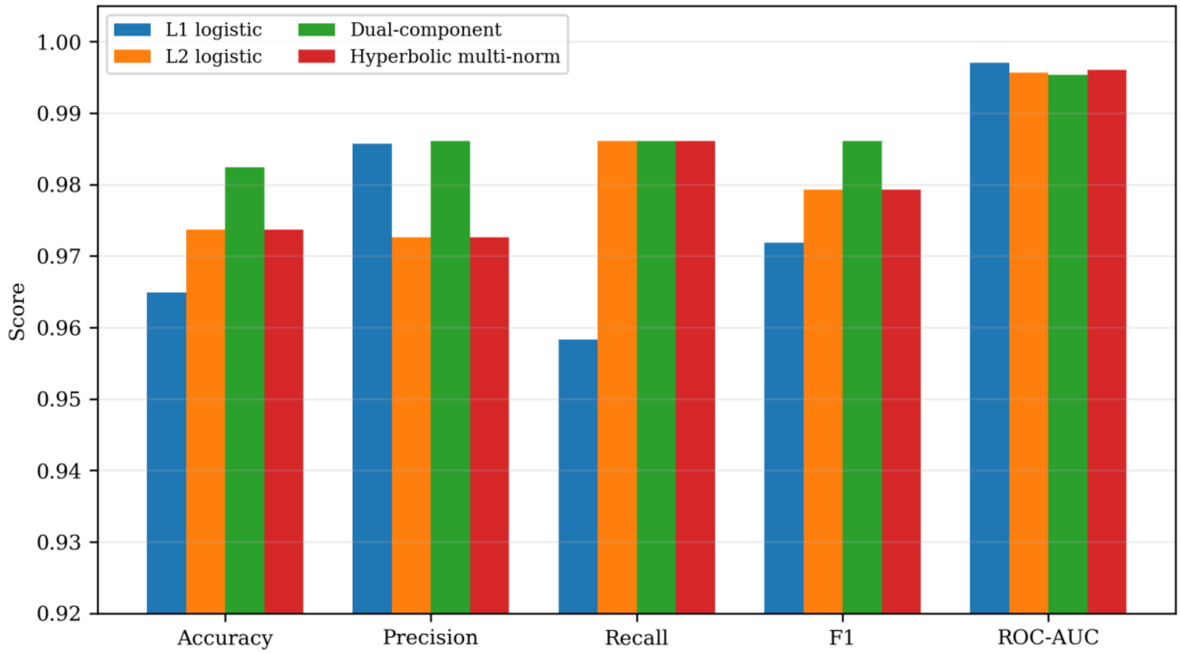

Figure 2. Test-set discrimination metrics for the four classifiers.

Noise results qualify the clean-data ranking. At σ=1.0, HMR retained 0.913 mean accuracy, marginally exceeding L2 (0.911) and more clearly exceeding the dual baseline (0.893). Its decline from zero noise was 0.061, compared with 0.063, 0.090 and 0.123 for L2, dual and L1. Noise and decline were strongly correlated for HMR ($r=0.990$, $p<0.001$), as expected for monotone degradation.

Table 4. Mean accuracy under increasing Gaussian perturbation (200 replicates)

Noise σ	L1	L2	Dual	HMR	HMR decline
0.00	0.965	0.974	0.982	0.974	0.000
0.10	0.966	0.974	0.974	0.974	0.000
0.25	0.948	0.964	0.965	0.963	0.011
0.50	0.919	0.952	0.945	0.952	0.022

0.75	0.882	0.933	0.920	0.934	0.040
1.00	0.842	0.911	0.893	0.913	0.061

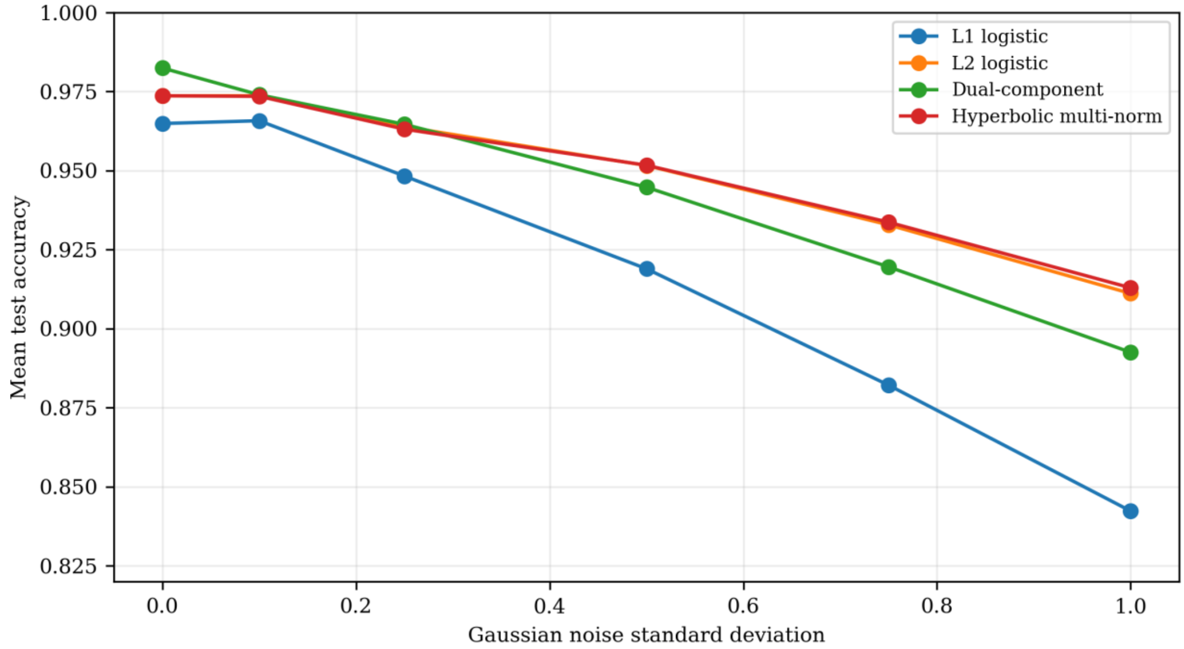

Figure 3. Mean classification accuracy as Gaussian perturbation increases.

Paired fold tests found no reliable advantage. HMR exceeded L1 by 0.011 on average, but the 95% interval crossed zero (p=0.394). HMR and L2 had identical fold scores; HMR and dual differed only in fold ordering. Figure 4 confirms stable numerical convergence within 28 L-BFGS iterations.

Table 5. Paired five-fold accuracy comparisons

Comparison	**Mean diff.**	**t**	**p**	**95% CI low**	**95% CI high**	**Cohen dz**
HMR vs L1 logistic	0.011	0.953	0.394	-0.021	0.043	0.426
HMR vs L2 logistic	0.000	0.000	1.000	0.000	0.000	0.000
HMR vs Dual-component	0.000	0.000	1.000	-0.010	0.010	0.000

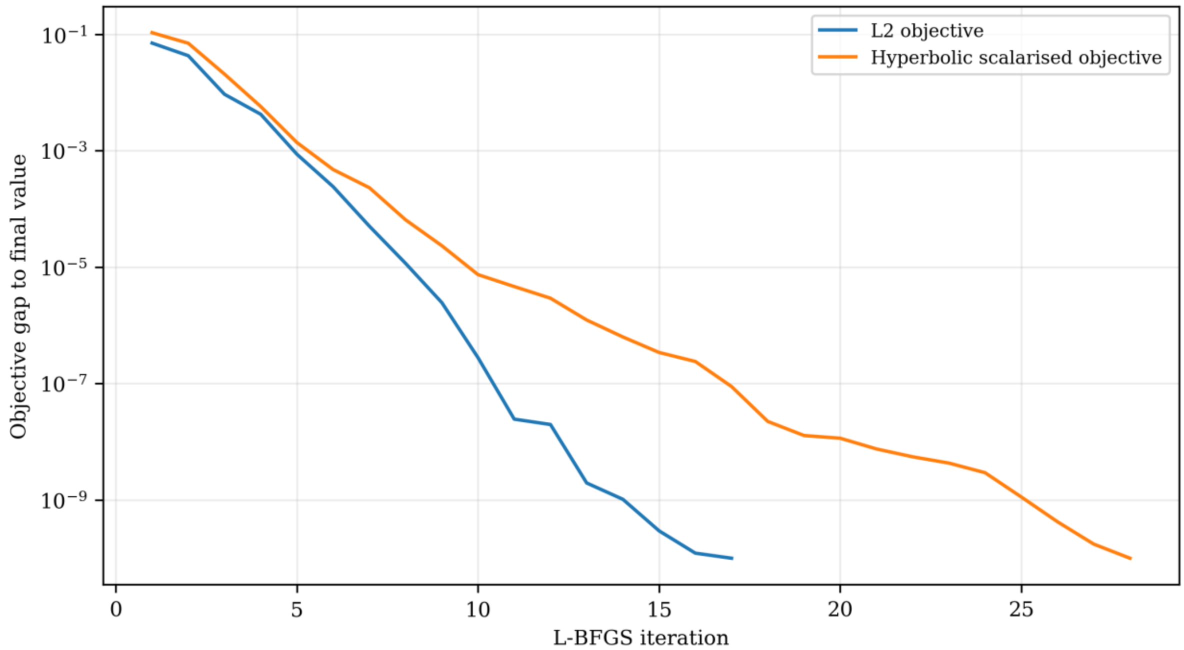

Figure 4. Optimisation convergence expressed as objective gap to the final value.

Discussion

The theoretical contribution links multinorm geometry with bicomplex idempotents. Since each component can be analyzed using familiar complex functional analysis, with hyperbolic order keeping both magnitudes, in this context, it takes the role of multiview regularization, one of the channels is the original geometry, and in the other, extremes are suppressed. Related complex-valued works also follow this logic and preserve paired structure instead of flattening it (Scardapane et al. 2020; Xu et al. 2023; Xu et al. 2025).

The study does not support a claim of omnipresent superiority. The dual baseline was the best in terms of accuracy and calibration on clean data, and HMR's contribution had the advantage of competitive cross-validation and a small high-noise advantage. The improvement could be the result of multiview group regularization rather than bicomplex arithmetic, therefore, ablation on component construction is required. Other issues are the order relation, selected scalarisation, one small medical dataset, high optimization time, and absence of developed bicomplex software. The most plausible areas of application are for multichannel signals, imaging, sensor fusion, multimodal diagnosis, and uncertainty-aware models, where paired components originate from interpretable structures.

Conclusion

This study defined hyperbolic multi-norms on bicomplex modules and used succinct decomposition methods to demonstrate that hyperbolic multi-norms can be built on bicomplex modules. Their topology and completeness coincide with that of two compatible complex multi-normed spaces. The idempotent representation further provided a constructive learning framework, where primary and strongly transformed features were simultaneously optimized under a scalarized hyperbolic framework. On the Breast Cancer Wisconsin Diagnostic dataset, HMR reached 0.974 accuracy, 0.979 F1 score, and 0.996 ROC-AUC, with a cross-validation accuracy of 0.982 ± 0.006. However, it did not outperform the dual-component classifier in clean data, and the paired comparisons were not statistically significant.

However, it claimed the least accuracy drop under intense Gaussian noise, with a slight edge over the L2 distance. Hence, hyperbolic multi-norms offer a comprehensive structure for dual-component learning and uncertainty learning. However, the current observations remain in the realm of preliminary. The following research lines should explore bicomplex kernels, hyperbolic neural networks, various scalarizations, and large multimodal datasets.

REFERENCES:

1. Alpay, D., Luna-Elizarrarás, M. E., Shapiro, M., & Struppa, D. C. (2014). Basics of functional analysis with bicomplex scalars, and bicomplex Schur analysis. Springer. https://doi.org/10.1007/978-3-319-05110-9
2. Alpay, D., Diki, K., & Vajiac, M. (2023). A note on the complex and bicomplex valued neural networks. Applied Mathematics and Computation, 445, 127864. https://doi.org/10.1016/j.amc.2023.127864
3. Dales, H. G., & Polyakov, M. E. (2012). Multi-normed spaces. Dissertationes Mathematicae, 488, 1–165. https://doi.org/10.4064/dm488-0-1
4. Değirmen, N., & Sağır, B. (2025). A new D-normed Banach bicomplex BC-module derived using matrix of hyperbolic Fibonacci numbers. WSEAS Transactions on Mathematics, 24, 203–208. https://doi.org/10.37394/23206.2025.24.20
5. Friedman, J. H., Hastie, T., & Tibshirani, R. (2010). Regularization paths for generalized linear models via coordinate descent. Journal of Statistical Software, 33(1), 1–22. https://doi.org/10.18637/jss.v033.i01
6. Ghosh, C., & Mondal, S. (2022). Bicomplex version of Lebesgue's dominated convergence theorem and hyperbolic invariant measure. Advances in Applied Clifford Algebras, 32, 37. https://doi.org/10.1007/s00006-022-01216-0
7. Kumar, R., & Saini, H. (2016). Topological bicomplex modules. Advances in Applied Clifford Algebras, 26, 1249–1270. https://doi.org/10.1007/s00006-016-0646-1
8. Lee, C. Y., Hasegawa, H., & Gao, S. C. (2022). Complex-valued neural networks: A comprehensive survey. IEEE/CAA Journal of Automatica Sinica, 9(8), 1406–1426. https://doi.org/10.1109/JAS.2022.105743
9. Luna-Elizarrarás, M. E., Panza, M., Shapiro, M., & Struppa, D. C. (2020). Geometry and identity theorems for bicomplex functions and functions of a hyperbolic variable. Milan Journal of Mathematics, 88, 247–261. https://doi.org/10.1007/s00032-020-00313-8
10. Luna-Elizarrarás, M. E., Shapiro, M., Struppa, D. C., & Vajiac, A. (2015). Bicomplex holomorphic functions: The algebra, geometry and analysis of bicomplex numbers. Birkhäuser. https://doi.org/10.1007/978-3-319-24868-4
11. Nguyen, K., Fookes, C., Sridharan, S., & Ross, A. (2023). Complex-valued iris recognition network. IEEE Transactions on Pattern Analysis and Machine Intelligence, 45(1), 182–196. https://doi.org/10.1109/TPAMI.2022.3152857
12. Pedregosa, F., Varoquaux, G., Gramfort, A., et al. (2011). Scikit-learn: Machine learning in Python. Journal of Machine Learning Research, 12, 2825–2830.
13. Scardapane, S., Van Vaerenbergh, S., Hussain, A., & Uncini, A. (2020). Complex-valued neural networks with nonparametric activation functions. IEEE Transactions on Emerging Topics in Computational Intelligence, 4(2), 140–150. https://doi.org/10.1109/TETCI.2018.2872600

14. Toksoy, E. (2024). Hyperbolic valued Beurling weighted bicomplex Lebesgue spaces and some of their geometric characteristics. Journal of Inequalities and Applications, 2024, 153. https://doi.org/10.1186/s13660-024-03238-7
15. Vieira, N. (2023). Bicomplex neural networks with hypergeometric activation functions. Advances in Applied Clifford Algebras, 33, 20. https://doi.org/10.1007/s00006-023-01268-w
16. Wolberg, W., Street, W., & Mangasarian, O. (1995). Breast Cancer Wisconsin (Diagnostic) [Dataset]. UCI Machine Learning Repository. https://doi.org/10.24432/C5DW2B
17. Xu, J., Wu, C., Ying, S., & Li, H. (2022). The performance analysis of complex-valued neural network in radio signal recognition. IEEE Access, 10, 48708–48718. https://doi.org/10.1109/ACCESS.2022.3171856
18. Xu, Z., Hou, S., Fang, S., Hu, H., & Ma, Z. (2023). A novel complex-valued hybrid neural network for automatic modulation classification. Electronics, 12(20), 4380. https://doi.org/10.3390/electronics12204380
19. Xu, Z., Fan, Y., Fang, S., Fu, Y., & Yi, L. (2025). A lightweight dual-branch complex-valued neural network for automatic modulation classification of communication signals. Sensors, 25(8), 2489. https://doi.org/10.3390/s25082489
20. Singh, N. (2018). Hyperbolic-valued multi-norms on Banach lattices. *International Journal of Advance Research in Science and Engineering, 7*(4), 163–173. https://www.ijarse.com/ADMIN/admin/postimages/images/fullpdf/1524055622_JK1532ijarse.pdf